Title

AN HREELS STUDY OF THE SURFACE STRUCTURE OF BENZENE ADSORBED ON THE Rh(lll) CRYSTAL FACE

Author

Koel, B.E.

Publication Date

1983-11-01

Lawrence Berkeley Laboratory
UNIVERSITY OF CALIFORNIA

Materials & Molecular Research Division

Submitted to the Journal of Physical Chemistry

AN HREELS STUDY OF THE SURFACE STRUCTURE OF BENZENE ADSORBED ON THE Rh(111) CRYSTAL FACE

B.E. Koel, J.E. Crowell, C.M. Mate, and G.A. Somorjai

November 1983

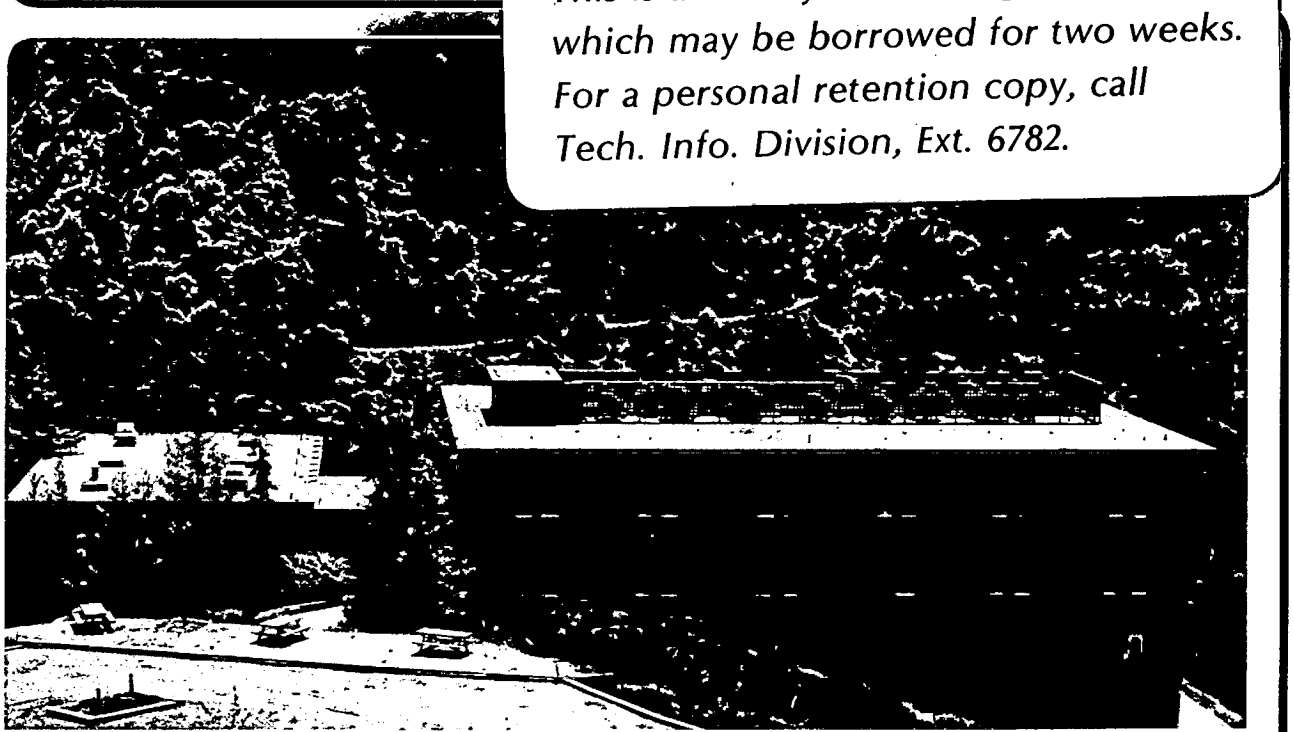

Prepared for the U.S. Department of Energy under Contract DE-AC03-76SF00098

DISCLAIMER

LBL-16012

AN HREELS STUDY OF THE SURFACE STRUCTURE OF BENZENE ADSORBED ON THE Rh(111) CRYSTAL FACE

B. E. Koel*, J. E. Crowell, C. M. Mate and G. A. Somorjai

Materials and Molecular Research Division
Lawrence Berkeley Laboratory, and
Department of Chemistry
University of California, Berkeley
Berkeley, CA 94720

* Miller Institute Postdoctoral Fellow
Present Address: Department of Chemistry, University of Colorado,
Boulder, CO 80309

ABSTRACT

Benzene adsorption on the Rh(111) crystal surface has been studied using HREELS, LEED and TPD. The vibrational spectra indicate that benzene adsorbs molecularly at 300K and is π-bonded to the surface with the ring plane parallel to the surface plane. Recent dynamic LEED calculations [1] together with the angle-dependent HREELS studies reported here establish a $C_{3v}(\sigma_d)$ bonding symmetry for the $c(2\sqrt{3}x4)rect\text{-}C_6H_6$ structure. Several other ordered benzene overlayers can be formed between 300-400K depending on the benzene coverage. No large changes occur in the chemisorption bonding mode or geometry coincident with the two-dimensional ordering phase transitions in this temperature range. The vibrational spectra show that two molecular adsorption sites can be populated. Benzene adsorption is only partially reversible; less than twenty percent of the adsorbed benzene desorbs molecularly upon heating. The remaining benzene irreversibly decomposes, evolving hydrogen and leaving a carbon-covered surface. The TPD and HREELS data on Rh(111) and other single crystal surfaces show correlations between the metal-benzene bond strength, the work function of the clean surface, and the frequency shifts of some of the molecular benzene vibrational modes.

1. Introduction

A molecular scale understanding of the structure and chemical bonding of aromatic molecules on metal surfaces is obtainable by employing the modern surface science techniques of high resolution electron energy loss spectroscopy (HREELS) and low energy electron diffraction (LEED). Detailed scrutiny of the bonding and reactivity at these metal-organic interfaces could help in unraveling the reaction steps during the catalytic conversion of aromatic molecules and could provide an understanding of the molecular basis for adhesion and lubrication.

This paper presents a detailed study of the chemisorption of one of the simplest aromatic molecules, benzene, on the (111) crystal face of rhodium. HREELS and LEED were used to study the molecular structure and bonding of chemisorbed benzene from 270-400K, below the onset of significant dehydrogenation or decomposition. We have obtained vibrational spectra of several ordered and disordered benzene monolayers in this temperature range in order to study the influence of two-dimensional phase transitions on the adsorption geometry, i.e. to determine if any large changes occur in the mode of bonding (di-σ-bonding vs. π-bonding) or in the bonding geometry (e.g., a compressional phase transition to give significantly tilted benzene molecules) up to the decomposition temperature [2]. The thermal decomposition of benzene will be discussed in an upcoming article relating the similar surface fragments produced upon annealing of alkene and benzene monolayers [3]. In the current study, the molecular adsorption

geometry and adsorption site symmetry is determined by use of the surface dipole selection rule in conjunction with angle-resolved HREELS data. Independent results from HREELS are compared to the surface structure and bonding site obtained from dynamic LEED calculations [1] to give a consistant picture of the adsorption site and benzene-metal surface bonding configuration.

Many spectroscopic studies [4-20] have concluded that benzene chemisorbs molecularly on transition metal surfaces with its ring plane parallel to the surface plane, bonding to the surface predominately through π-orbitals. Angle-resolved photoemission studies [4-7] indicate a flat-lying orientation of benzene and show chemical shifts of the bonding π-orbital. Vibrational spectroscopy of benzene chemisorbed on both single crystal [8-14] and supported metal surfaces [15-17] show that benzene is oriented with its ring plane parallel to the surface plane and is only weakly distorted from the gas phase molecular structure upon adsorption, indicating π-bonding. Temperature programmed desorption (TPD) studies [8-10, 18-20] indicate that benzene adsorption is associative on many transition metal surfaces at 300K, but only partially reversible. We have correlated the surface chemistry of benzene on Rh(111) with the previous studies on other metal surfaces.

2. EXPERIMENTAL

The experiments were performed in an ultra-high vacuum chamber which has ion, titanium sublimation, and diffusion pumps with a base pressure of below 1×10^{-10} torr. The chamber, described previously

[21], is built on two levels with AES, LEED, TPD and sputtering capabilities in the upper level and HREELS in the lower level. The sample is moved from one level to the other (~15 cm) by an extremely stable manipulator with the X-Y position of the sample monitored precisely by travel gauges.

The spectrometer used for HREELS is similar to designs commonly used [22], and consists of two identical 35 mm cylindrical sectors which have 0.20 mm x 4.0 mm slits as the entrance and exit apertures. The incident current at the crystal is 1×10^{-10} A. The sectors are typically operated at 0.5 eV pass energy, which for specular reflection of a 3.5 eV incident beam from a clean Rh(111) surface yields a total system resolution (FWHM of the elastic peak) of 48 cm^{-1} (6 meV) and a counting rate of 4×10^5 cps for the elastic peak. The incident energy was ~4 eV referenced to the sample vacuum level. The total scattering angle is fixed at 120°, so that for specular reflection $\theta_i = \theta_s = 60°$ from the surface normal. Off-specular ($\theta_i \neq \theta_s$) measurements were performed by rotation of the sample about an axis perpendicular to the scattering plane. Off-specular measurements varied up to 20° from specular reflection, with θ_i varying between 55 and 70°. The angular FWHM of the detected elastic peak for the above conditons is ~4°. The power supply used for supplying the spectrometer voltages is extremely stable and noise-free, and has been described in detail elsewhere [23].

The Rh(111) sample was cleaned in the chamber using a combination of Ar^+ sputtering (0.5-1 kV, 8 μA), annealing at 1000-1400K in vacuum, and oxygen treatments (3×10^{-7} torr, 950-1250K). Contaminants initially observed were sulfur, boron, carbon, and oxygen. AES, LEED and HREELS were used to insure that the surface was clean and well-ordered. We initially observed vibrations in the HREEL spectrum similar to that reported by Semancik et al. [24] due to boron plus oxygen surface impurities and subsequently we were careful to remove surface boron. The crystal temperature was measured by a chromel-alumel thermocouple spot-welded to the crystal.

Spectral grade benzene (99.9 percent, Fischer) and fully deuterated benzene-d_6 (99 atom percent D, Norell Chemical) were stored over calcium hydride and used without further purification. Sample dosing was done by backfilling the chamber or by using a multichannel array nozzle doser. The doser has an enhanced exposure rate of five times the backfilling rate. All exposures cited are uncorrected for ion gauge sensitivity.

3. Results and Interpretation

3.1 Temperature Programmed Desorption (TPD)

Benzene adsorption occurs on Rh(111) at 300K with an initial sticking coefficient of near unity, as indicated by AES and TPD. The sticking coefficient is constant ($S = S_0$) for benzene coverages ($\theta_{C_6H_6}$) less than 85 percent of the saturation amount. Saturation coverage is nearly reached after 5L exposure, but the coverage can be

increased about 15 percent by exposures of 70L. The saturation benzene coverage on Rh(111) at 300K and at 5 x 10^{-10} torr, as determined from the sharp c(2$\sqrt{3}$x4)rect LEED pattern (assuming one molecule per unit cell), is 0.125 ML (ML = monolayer, defined relative to the surface Rh atom density of 1.60 x 10^{15} atoms/cm^2), corresponding to a carbon atom coverage (θ_C) of 0.75 ML [25].

Figure 1 shows TPD spectra for (A) C_6H_6 desorption after C_6H_6 exposure and (B) D_2 desorption following C_6D_6 exposure of Rh(111) at 300K. The chemisorption of benzene at less than about 25 percent of saturation coverage ($\theta_{C_6H_6}$ < 0.03 ML) is thermally irreversible. No detectable molecular benzene thermal desorption occurs at low coverages, only dehydrogenation yielding H_2 desorption and an adsorbed hydrocarbon fragment. Some reversible benzene chemisorption occurs for exposures larger than 2L, and this amount increases with increasing exposure. For exposures greater than 2L, molecular benzene desorption occurs immediately upon heating and continues until 500K. After a 5L exposure, a broad benzene desorption peak is observed at 415K, which shifts to 395K after saturation exposure. TPD spectra for desorption of C_6D_6 from Rh(111) after C_6D_6 exposure are identical to those in Figure 1A. The benzene desorption peak shift can be explained by repulsive interactions between benzene molecules at high coverages (reducing the adsorption energy with increasing coverage) or the existence of overlapping desorption states with different desorption energies. These two effects are difficult to distinguish, but later we will show evidence for two adsorption states using HREELS.

AES, along with supporting evidence from HREELS and LEED, indicates that heating the benzene saturated surface to 380K (which removes about one-half of the molecular desorption peak) reduces the adsorbate coverage less than ten percent. Therefore, at high coverages molecular benzene desorption competes with dehydrogenation during heating of the surface, but still accounts for less than 0.02 ML C_6H_6.

Figure 1B shows the TPD spectra for D_2 following C_6D_6 exposure to Rh(111) at 300K. TPD spectra for H_2 after C_6H_6 exposures were qualitatively the same. An isotope effect was apparent for the largest desorption peak (473K) which occurred at 20K lower temperature for H_2 evolution. Also, some small amount of contaminant coadsorbed hydrogen that desorbed near 370K was observed for small benzene coverages. In Figure 1B several D_2 desorption states are observed between 430-540K after small exposures. Increasing exposure caused the dominant peak at 495K to increase in size and, at coverages greater than 50 percent of saturation, to shift gradually to lower temperatures. The peak temperature reached a minimum of 475K at saturation. Also, with increasing exposure, the peak at 540K grows in intensity and broadens to higher temperatures. At saturation coverage, D_2 desorption continues to nearly 800K, with a slight peak near 700K.

The dominant D_2 or H_2 desorption peak corresponds to initial dissociation of hydrogen from molecular benzene; the tail of continuous hydrogen evolution following this peak is due predominately to hydrogen dissociation from the remaining hydrocarbon fragments [3]. The broadening of this desorption state to higher temperatures with

increasing coverage is likely due to a higher activation energy for C-H bond scission as more dissociation sites become occupied.

3.2 Low Energy Electron Diffraction (LEED)

Adsorption of benzene on Rh(111) between 270-320K initially caused diffuse fractional-order spots to appear between 1-3L exposure, but a large background intensity still indicated considerable surface disorder. The fractional-order spot intensity increased with further exposure so that after 10L, several ordered LEED structures could be identified. The quality of the patterns could often be improved by large exposures of 30-70L and annealing. The particular pattern observed depended sensitively on the benzene coverage, which is a function of the benzene exposure, benzene background pressure, and sample temperature. We have observed patterns denoted as $(2\sqrt{3} \times 3)$rect, (3×3), c$(2\sqrt{3} \times 4)$rect and $(\sqrt{7} \times \sqrt{7})$R 19.1°. The "rect" notation indicates a rectangular unit cell. In matrix notation, these LEED patterns are labelled respectively $\begin{pmatrix} 3 & 3 \\ \bar{2} & 2 \end{pmatrix}$, $\begin{pmatrix} 3 & 0 \\ 0 & 3 \end{pmatrix}$, $\begin{pmatrix} 3 & 1 \\ 1 & 3 \end{pmatrix}$ and $\begin{pmatrix} 3 & 2 \\ 1 & 3 \end{pmatrix}$. The patterns are all related by small changes in coverage, and are given in order of increasing coverage. These results are consistent with previous results reported by Lin et al. [25] where they discuss in detail the c$(2\sqrt{3} \times 4)$rect and (3×3) structures, and did not choose to discuss the other structures sometimes encountered.

3.3 High Resolution Electron Energy Loss Spectroscopy (HREELS)

The HREEL spectra of benzene adsorbed on the Rh(111) crystal face shown in Figure 2 were obtained for specular scattering at a

saturation benzene coverage under conditions that produced a well-ordered c($2\sqrt{3}$ x 4)rect LEED pattern. The dominant features are the 345 and 810 cm^{-1} losses observed for C_6H_6 (Figure 2A) and the 330 and 565 cm^{-1} losses observed for C_6D_6 (Figure 2B). From the isotopic shifts observed for these spectra, the losses at 810, 1130, and 3000 cm^{-1} are identified as C-H vibrations and those at 345, 550, 1320 and 1420 cm^{-1} as Rh-C and C-C vibrations. Contamination of the Rh(111) surface by 0.01 ML CO coadsorption produced a loss peak near 1660 cm^{-1}, which is assigned to the CO stretching frequency (ν_{CO}) of bridge-bonded CO [26].

The vibrational frequencies for chemisorbed benzene are given in Table 1 along with the mode number and symmetry representation of the corresponding vibrational modes in free benzene. This assignment relies on guidance from calculations in which the valence force field of $Cr(C_6H_6)(CO)_3$ was transferred to chemisorbed benzene on Raney nickel [17]. These calculations showed that ν_9 and ν_{13} would shift to 1253 cm^{-1} and 1439 cm^{-1}, respectively, upon chemisorption. Our assignment is in agreement with work on Ni(111) by Bertolini and Rousseau [8] where they assigned peaks at 1325 and 1425 cm^{-1} to ν_9 and ν_{13}, respectively. Lehwald et al. [13] assigned the peak at 1420 cm^{-1} on Pt(111) and 1430 cm^{-1} on Ni(111) to ν_9 and did not identify a peak near 1320 cm^{-1}. An additional mode at 835 cm^{-1} in the C_6D_6 spectrum in Figure 2B is too intense to be exclusively due to a δ_{CD} loss (ν_{10}) and is additionally assigned in Table 1 to a molecular ring stretch (ν_2).

This loss is difficult to see for C_6H_6 on-specular, as in Figure 1A, since it is obscured by the intense γ_{CH} loss peak. However, this mode can be observed for C_6H_6 in off-specular HREELS spectra (e.g., Figure 7).

The vibrational spectra establish that benzene is molecularly chemisorbed. The frequency of the CH out-of-plane bending mode (γ_{CH} is about the same as in metal-benzene complexes which are known to have molecular benzene π-bonded to the metal atom(s), e.g. γ_{CH} = 795 cm^{-1} for $(C_6H_6)_2Cr$ [27]. Furthermore, chemisorbed benzene is oriented so that the molecular ring plane is parallel to the metal surface plane. This geometry is established by comparing the infrared absorption spectra of free benzene in the gas [28] or liquid phase [29] with the HREELS spectra in Figure 2, and by using the surface dipole selection rule [30]. Infrared active fundamentals for free benzene involving dynamic dipole moments parallel to the molecular ring plane (ν_{12}, ν_{13}, and ν_{14}; E_{1u} symmetry) and perpendicular to the ring plane (ν_4; A_{2u} symmetry) have similar intensities. The detection in Figure 2A of an intense γ_{CH} mode, derived from ν_4 with A_{2u} symmetry, and the weak intensity of the E_{1u} modes is due to the "flat" orientation of benzene on the Rh(111) surface and the conditions of the dipole selection rule: only vibrational modes with dynamic dipole moments perpendicular to the surface are observed as dipole-active. Further discussion of this selection role and its use in determining the adsorption symmetry from the observed vibrational modes is given in the appendix. Additionally,

confirmation of this geometry is given by angle-dependent HREEL spectra discussed in Section 3.4. As we shall now show, this general molecular orientation of the benzene molecular ring plane parallel to the Rh(111) surface in the c($2\sqrt{3}$ x 4)rect structure also occurs under all conditions of coverage and temperature studied, up to the start of significant benzene decomposition.

Vibrational spectra shown in Figure 3 were obtained for disordered benzene overlayers at coverages less than saturation and show only minor differences from Figure 2 in the relative intensities of the in-plane and out-of-plane modes. This data confirms a similar adsorption geometry for these cases also. The spectra taken after 0.5L and 1.5L exposure show strong losses due to contaminant CO: ν_{CO} at 2030-2015 cm^{-1} and a metal-carbon stretching vibration (ν_{Rh-CO} = 485 cm^{-1}), both characteristic of linearly-bonded CO. Benzene exposures larger than 1.5L greatly reduce the amount of CO present and shifts the co-adsorbed CO to a bridge-bonded site with ν_{CO} = 1710-1676 cm^{-1}. The $\nu_{Rh-C_6H_6}$ mode at 550 cm^{-1} is partially obscured, but does seem to increase in intensity with increasing benzene coverage. The lowest energy $\nu_{Rh-C_6H_6}$ mode changes little in intensity, but shifts from 330 cm^{-1} to 345 cm^{-1} with increasing benzene coverage. The weak loss intensity between 900-1500 cm^{-1} shows no significant changes in relative intensity or energy of the vibrational modes in this region as a function of coverage.

The γ_{CH} and ν_{CH} modes both shift and broaden with increasing benzene coverage. At low coverage, the ν_{CH} loss peak occurs at

3030 cm^{-1} with a FWHM of ~55 cm^{-1} and the γ_{CH} loss appears as a narrow peak at 790 cm^{-1}. At saturation coverage, the ν_{CH} loss peak broadens to ~100 cm^{-1} FWHM with the center at 2995 cm^{-1}, while the γ_{CH} peak also braodens and shifts to 815 cm^{-1}. We can account for these spectral changes by a model that includes the presence of benzene in a new adsorption site which is occupied above 2L exposure (also the onset of molecular benzene desorption) that is characterized by a higher energy γ_{CH} mode and lower energy ν_{CH} mode than benzene that adsorbs initially. The peaks due to the second site appear as shoulders at intermediate coverages and dominate the spectrum near saturation coverage.

The vibrational spectra are also very similar irrespective of the degree of ordering or the particular ordered structure present, indicating again that the benzene adsorption geometry is similar under all of these conditions. Figure 4 shows specular HREEL spectra of benzene adsorbed in the c($2\sqrt{3}$ x 4)rect and (3x3) structures. The (3x3) layer was obtained by momentary warming of the c($2\sqrt{3}$ x 4)rect benzene layer to 393K and waiting several hours in vacuum. Besides small changes in relative intensities and an overall decrease in total intensity for the (3 x 3) layer, no large changes occur in the vibrational spectra as the surface two-dimensional structure is altered. The increase in frequency of ν_{CO} for bridge-bonded CO from 1660 to 1710 cm^{-1} and the additional ν_{CO} mode at 1960 cm^{-1} for linearly-bonded CO occur because the surface was exposed to the background (mostly CO) for a prolonged period, and additional clean surface

sites become available as molecular benzene desorbs upon warming the surface to 393K (see Figure 1A). The small changes in frequency observed for the benzene modes are also seen for unstructured layers produced at subsaturation exposures, as is evidenced in Figure 3. Adsorption conditions that result in a surface which gives a poor LEED pattern (considerable surface disorder) result sometimes in slight shifts of the γ_{CH} and ν_{CH} losses in HREELS and small increases in the relative intensity of the loss peaks at 1130 and 1420 cm^{-1}.

The small changes in frequency observed for the benzene γ_{CH} and ν_{CH} modes in Figure 4 are similar to those seen for unstructured layers produced at subsaturation exposures in Figure 3. This led to an investigation of the γ_{CH} and ν_{CH} regions at higher resolution. Figure 5 shows that at saturation coverage, the γ_{CH} peak near 810 cm^{-1} in Figures 2, 3 and 4 is actually composed of two peaks of frequencies 776 and 819 cm^{-1}, when observed with a resolution of 27 cm^{-1} (FWHM). Similarly, two ν_{CH} peaks are observed at ~2970 cm^{-1} and 3020-3030 cm^{-1}. At low coverages the intensity ratios (I_{776}/I_{819}) and (I_{3030}/I_{2970}) are clearly greater than 4, but decreases to ~0.3 at saturation coverage. These ratios change again to ~1.6 as the saturation layer is warmed to 390K. These results indicate the presence of two benzene chemisorption states that are populated to different degrees dependent on benzene coverage and the surface temperature, but which show little variation in the molecular bonding geometry. The very small splitting (43 cm^{-1}) of the γ_{CH} loss peaks resulted previously in an incorrect conclusion that only one adsorption site was occupied on Rh(111) [2].

The spectra in Figures 3 and 4 indicate that weak adsorbate-adsorbate interactions, either direct or thru-metal, are responsible for the two-dimensional order-order transitions and show that no major changes result in the bonding mode or geometry at the surface. Furthermore, HREEL spectra taken after very large exposures (>300L) show that (1) no compressional phase transition, such as that observed for pyridine on Ag(111) [31], occurs for our conditions to produce two different bonding geometries of benzene near 300K, and that (2) no evidence was found for a significant coverage of benzene adsorbed with its ring inclined to the surface, as suggested might be possible on Pt(111) for the benzene C($2\sqrt{3}$ x 5)rect structure obtained after similar large exposure [32].

3.4 The Structure of Benzene Chemisorbed on Rh(111): c($2\sqrt{3}$x4)rect-C_6H_6/Rh(111)

Angle-dependent HREELS studies are required to determine with certainty which vibrational modes of chemisorbed benzene are dipole-active, since it is possible for impact scattering and dipole scattering mechanisms to give contributions of comparable magnitude for weak loss peaks in the specular direction [33]. The results of such an angular profile study for c($2\sqrt{3}$x4)rect-C_6H_6 on Rh(111) shown in Figure 6. Representative specular and off-specular HREEL spectra for this case are also shown in Figure 7. In moving from a specular to 15° off-specular scattering geometry, the 1130, 1320, 1420 and 3000 cm^{-1} modes decrease in intensity by factors of 1.3-2.6, while the modes at 345, 550, and 810 cm^{-1} decrease by a factor of

8-18, compared to a decrease of 150-170 in the elastic peak. From the intensity variation of these losses with angle, it is clear that all seven losses have dipole scattering contributions. However, all modes, except possibly the 550 cm^{-1} vibration, also have impact scattering contributions to the signals detected for specular scattering. This impact contribution is substantial (40-70 percent) for the modes occurring at 1130, 1320, 1420 and 3000 cm^{-1}. Many additional vibrational modes, with only small intensities due to weak impact scattering account for the additional intensity seen for off-specular scattering in Figure 7 between 700-1000 cm^{-1} and 1300-1500 cm^{-1}. These losses are not well-resolved and are not assigned in Table 1.

We can determine the symmetry of the surface complex (molecule plus adsorption site) by using the assignments of the dipole-active modes for chemisorbed benzene and considering the correlation table for the symmetry point group of gas phase benzene, D_{6h} [30,34]. A correlation table makes use of the relationships between the representations of D_{6h} and its subgroups to allow us to predict which vibrational modes would be observed to be dipole-active in HREELS upon reduction of the D_{6h} symmetry. The surface dipole selection rule in HREELS allows only those modes with totally symmetric representations (A_1, A' and A) to be dipole-active. In addition to these modes, new dipole-active vibrations (ν_{Rh-C}) may also result from removing the translational and rotational degrees of freedom when the benzene molecule becomes fixed in space upon adsorption.

Adsorption on the Rh(111) surface removes at least the σ_h symmetry plane to give C_{6v} symmetry for the surface complex and causes only the modes with A_{1g} and A_{2u} symmetry in free benzene to become dipole-active. If the adsorption is centered over a hollow site or if second layer interactions are important for atop site adsorption, the symmetry is further reduced to C_{3v}. The dipole scattering contribution to the modes at 1130 and 1320 cm^{-1} establishes that the adsorption site symmetry is $C_{3v}(\sigma_d)$. This point group implies that the symmetry planes of the Rh(111) substrate bisect the dihedral angles between planes that include adjacent CH bonds of the ring. Due to the small number of dipole-active modes observed, we can rule out adsorption with lower symmetries that might result from asymmetric distortion of the benzene molecule due to bonding, adsorption centered over a less symmetric surface site, or significant tilting of the molecular ring plane with respect to the surface. These arguments are presented in more detail in the appendix.

Other work has also concluded that benzene adsorbed on Ag(111) [12], and Ni(111) and Pt(111) [13] occupies adsorption sites of C_{3v} (σ_d) symmetry. However, Haaland [15] suggests benzene symmetrically distorts to this geometry on alumina supported platinum, rather than strictly adsorbing on a site of this symmetry. An inspection of Table 2 suggests that C_{3v} (σ_d) adsorption symmetry is reasonable for all the metal surfaces studied to date. Clearly such symmetry is not possible for adsorption on either Ni(100) or Ni(110). Correlation tables show that several additional modes should be dipole active for

C_{2v} symmetry (the highest symmetry point group expected on these crystallographic orientations). Why these modes are not seen is yet to be understood.

Our data is consistant with C_{3v} (σ_d) local symmetry for both benzene adsorption sites that can be populated on Rh(111). There are three possible sites that might have $C_{3v}(\sigma_d)$ symmetry: fcc hollow, hcp hollow, and atop. These sites could easily have different binding energies that would result in different characteristic vibrational energies. This same conclusion was also reached for Ni(111) and Pt(111) studies [13].

A model for the structure of the benzene monolayer deduced from dynamical LEED calculations for the I-V profiles of the c($2\sqrt{3}$ x 4) LEED pattern is shown in Figure 8 [1]. This model is supported by our determination of the adsorption geometry with the benzene ring parallel to the surface with surface symmetry C_{3v} (σ_d). The LEED calculations indicate bonding on a 3-fold hollow site with a second layer atom directly underneath (hcp hollow), while the HREELS data indicates two adsorption sites of C_{3v} (σ_d) symmetry and cannot be used to directly determine the identity of the sites. Taken together, the data suggests two of the three possible adsorption sites having C_{3v} (σ_d) symmetry are occupied at saturation coverage, with most of the benzene molecules centered over hcp-type hollow sites i.e. a large fraction, roughly 70 percent, of molecules have ν_{CH} = 819 cm^{-1} at saturation. The remaining benzene molecules (with ν_{CH} = 776 cm^{-1}) occupy either an fcc-type hollow or an atop site.

It is interesting to note that, an in-plane distortion of the benzene ring, as shown at right in Figure 8, gave the best fit between dynamic LEED theory and the experimental I-V profiles. Such a symmetric distortion would be consistent with the HREELS data as long as the distortions were symmetric. In fact, the vibrational spectra of benzene and the low temperature phase of acetylene are quite similar for several metal surfaces [33,35,36]. Lehwald et al. [13] have pointed out that the $\pi/di-\sigma$ bonding of acetylene over hollow sites found on Pt(111) [35], and also on Pd(111) [33], puts the C and H atoms into the same local geometry as expected for benzene over hollow sites, possibly with the same distortion. The observed production of benzene upon trimerization of acetylene on Ni [36] and Pd [37,38] surfaces gives additional reason to seriously consider the distortion calculated.

4. DISCUSSION

The surface chemistry of benzene adsorption on Rh(111) is similar to that observed previously on Pt and Ni surfaces. There are some differences, but a useful, representative picture of Group VIII metal-arene chemistry can probably be obtained by a detailed study of any one of these systems.

On Rh(111), a chemisorption state that is thermally irreversible is initially formed upon benzene exposure at 300K. This is also seen for benzene adsorption on Ni(111) [18], Pt(111) [19], Pt(100) [20], Ni(110) [9] and $Pt_{10}Ni_{90}$(111) [9]. The HREEL spectra show that benzene is molecularly adsorbed in this state. In addition, on Ni(111) [18] and

Pt(111) [19], no reversible H-D exchange for this state is observed. At higher coverages, a reversible chemisorption state can also be populated. Differences in the bonding of these two states on Rh(111), Ni(111) [13], and Pt(111) [13], is detected by HREELS studies that show two γ_{CH} vibrations with varying intensity ratios. The dependence of the relative intensity of these vibrations at loss peaks on coverage and temperature (concurrent with no other changes in the HREEL spectra) suggests that benzene adsorbs in two different sites on all of these surfaces. Infrared spectra of metal-arene complexes formed by co-condensing transition metal vapors with benzene at 77K or in argon matrices at 10K [27] show that when benzene is attached to small metal aggregates instead of a single metal atom, the γ_{CH} mode decreases in frequency by 15-45 cm^{-1}. This suggests that the lower frequency γ_{CH} mode, which is initially observed at low coverage, is due to benzene adsorption in a higher coordination site.

On Rh(111) only the low frequency γ_{CH} mode is detected at low coverages, with the two γ_{CH} modes seen at higher coverages separated by 43 cm^{-1}. Similar behavior is seen on Ni(111), but in this case the two modes are separated by 90 cm^{-1}. The low frequency mode is more intense at low coverages, but at high coverages the high frequency mode is the dominant loss peak, as on Rh(111). On Pt(111) the two γ_{CH} modes are also separated by 90cm^{-1}, but are equally intense at low coverage, which is different than observed for Ni(111) and Rh(111). TPD from Pt(111) also shows differences from Ni(111) and Rh(111) results. At low coverages, benzene both decomposes and desorbs

molecularly from a single high temperature state at 473-493 K [19]. At high coverages on Pt(111) the low frequency γ_{CH} mode is four times more intense than the high frequency mode, and an additional molecular desorption state at 373-403K is observed in TPD. The general surface chemistry of benzene on these three surfaces is similar, but Rh(111) and Ni(111) are most alike in the observed γ_{CH} frequencies and in the coverage dependence of the loss intensities in HREELS. This suggests that a similar site occupancy and surface structure may occur on Rh(111) and Ni(111). More studies on other metal surfaces are required to make certain possible correlations between adsorption sites, the tendency for molecular desorption, or decomposition and the γ_{CH} mode frequency.

The bending vibration for CH groups present in gas phase molecules is a strong function of the hybridization of the carbon atom, increasing in frequency with increasing hybridization, $sp < sp^2 < sp^3$ [28]. Similar trends are seen in metal-benzene complexes where the CH out-of-plane bending mode (γ_{CH}) frequency was found to increase in the order: nickel < cobalt < iron < chromium [27]. The CH mode is the most intense in the spectrum and undergoes substantial shifts, hence this bend has been used previously as an indirect means of relating metal-ring bond strengths for both arene- and cyclopentadienyl-metal complexes [39]. We would like to extend this correlation to metal surfaces.

The available TPD data for benzene and hydrogen evolution from chemisorbed benzene on single-crystal surfaces is given in Table 3.

First order desorption kinetics and a preexponential factor of $10^{13} sec^{-1}$ [40] were used in order to calculate the heats of desorption and to account for the different heating rates used in TPD, and thus facilitate comparisions among the different surfaces. The actual reaction order and preexponential factor should be similar on these surfaces, so that the above assumption results in only a small relative error.

The vibrational data for benzene adsorption on metal single-crystal surfaces is summarized in Table 2. The perturbation from gas phase benzene increases as one moves down the Table, toward higher frequency γ_{CH} vibrations. For the limited number of metals studied, the γ_{CH} frequency correlates reasonably well with the heat of desorption of molecular benzene, as shown in Figure 9. Thus, on metal surfaces, as in gas phase molecules and in metal-benzene complexes, the γ_{CH} frequency increases as the metal-benzene interaction becomes stronger.

This correlation is clearly not as simple as one would like; the frequency of the γ_{CH} is sensitive to both the metal-benzene interaction and the nature of the adsorption site. For example, on Rh(111) the lower frequency γ_{CH} mode (along with the higher frequency ν_{CH} mode) is observed at low coverages, while the higher frequency γ_{CH} mode (and lower frequency ν_{CH} mode) is observed at high coverages. By the above correlation, we would conclude that the benzene initially chemisorbed was perturbed the least, with the weakest metal-benzene chemisorption bond, compared to the benzene chemisorbed near saturation

coverage. This is contrary to our TPD data which shows that the initial benzene chemisorption state irreversibly decomposes thermally, while at saturation coverage some molecular benzene desorption occurs indicating weaker benzene-metal bonding at higher coverages. The decomposition of benzene on the surface is complex and the above effect in TPD could be due to a higher activation energy barrier to C-H bond scission because of the relative unavailability of metal-H or metal-fragment bonding sites at high benzene coverages, rather than a metal-benzene bonding difference. However, conventional thinking would also suggest that chemisorption bonding, in general, is strongest at low coverages. Thus, while a general trend of higher γ_{CH} frequency with greater metal-benzene interaction exists from metal to metal, the γ_{CH} frequency also depends on the nature (e.g., coordination number) of the adsorption site. This influence was alluded to earlier when we discussed results of infrared studies of metal-arene complexes that showed decreases in the γ_{CH} frequency of 15-45cm^{-1} due to higher coordination of the benzene [27]. The origin of this influence is that vibrational frequencies are determined by the shape of the potential well, not only by the depth of the potential well.

Other dipole-active modes given in Table 2 also show reasonable trends from one metal to another as the strength of the metal-benzene interaction increases. Inspection of Table 2 shows that in addition to the γ_{CH} vibrations, both M-C vibrations (ν_{M-C}) increase as the interaction with the surface increases. A similar trend was also

reported for benzene π-complexed to nickel, cobalt, iron, and chromium [27], with the metal-benzene interaction and ν_{M-C} increasing in the order given. The remaining three modes in Table 2 all decrease from their gas phase values upon chemisorption. The trend is clear that the magnitude of this decrease grows as one moves down the table, again indicating larger deviation from the gas phase with stronger adsorption. The frequencies observed for these modes give further information on the chemical state of chemisorbed benzene, e.g. the extent of rehybridization. The ring stretch and deformation mode (δ_{CC}) decreases by 30-40 cm^{-1} for π-complexed benzene [27], and between 45-60 cm^{-1} typically for all surfaces, but Ag(111), in Table 2. Furthermore, ν_{CH} typically decreases by 30-60 cm^{-1} from the gas phase value (3062 cm^{-1}) for adsorbed benzene. Comparing these values to the ν_{CH} of gas phase cyclohexane (2930 cm^{-1}) [28] and adsorbed cyclohexane on Ni(111) and Pt(111) (2900 cm^{-1} on both surfaces [41]) we conclude that benzene is rehybridized but still retains principally sp^2 character. Direct hydrogen-metal interaction does not occur in these single crystal metal-benzene systems since a large decrease in the CH stretching vibration is typically associated with such an interaction, and this is not observed for benzene adsorption (cf. ν_{CH} for organometallics containing C-H-M bonding occurs between 2350 and 2700 cm^{-1} [42]).

The degree of interaction between benzene and the first row transition metal atoms has also been correlated to the ability of these metals to serve as acceptors of π-electron density [43]. This

ability can be related to the electronegativity of the metal. The surface equivalent is the work function, and such a correlation exists for benzene chemisorption on metal surfaces, as shown in Figure 10. The bond-strength between benzene and a metal surface increases for higher work function surfaces, as can be indirectly measured from the increase in the CH out-of-plane bending frequency.

5. CONCLUSIONS

Benzene is associatively adsorbed on Rh(111) at 300K. HREEL spectra establish that benzene is chemisorbed with the molecular ring plane parallel to the metal surface plane and with a similar geometry for all of the ordered and disordered monolayers studied up to the temperature of decomposition. Two adsorption sites are observed, and the relative population of these depends on both temperature and coverage. Together, dynamic LEED calculations and the vibrational data indicate that at near saturation coverates a dominant fraction of benzene molecules occupy hcp hollow sites with $C_{3v}(\sigma_d)$ symmetry. Similar adsorption behavior and surface chemistry is seen for benzene chemisorbed on several other transition metal surfaces, including evidence for two adsorption sites with $C_{3v}(\sigma_d)$ symmetry.

The frequency of the CH out-of-plane bending mode (γ_{CH}) is an indirect indication of the extent of interaction between benzene and the metal surface. For the several transition metal single crystal surfaces studied so far, the strength of the metal-benzene bonding estimated by the metal-ring vibrational frequencies or the molecular desorption temperatures is correlated reasonably well with the

frequency shifts of the ν_{CH} vibration and also with the work function of the surface. However, the ν_{CH} mode is shown to be sensitive to the nature of the adsorption site, in addition to the chemisorption bond strength.

ACKNOWLEDGEMENTS

This work was supported by the Director, Office of Energy Research, Office of Basic Energy Sciences, Materials Sciences Division of the U.S. Department of Energy under Contract No. DE-AC03-76SF00098. Helpful conversations with Lin Rongfu, R. J. Koestner, and M. A. Van Hove are gratefully acknowledged. B.E.K. acknowledges the support of the Miller Institute for Basic Research in Science in the form of a Miller Fellowship.

REFERENCES

1. M. A. Van Hove, R. F. Lin, and G. A. Somorjai, Phys. Rev. Lett. 51, 778 (1983).
2. B. E. Koel and G. A. Somorjai, J. Electron Spectroc. Relat. Phenom. 29, 287 (1983).
3. B. E. Koel, J. E. Crowell and G. A. Somorjai, in preparation.
4. D. R. Lloyd, C. M. Quinn and N. V. Richardson, Solid State Commun. 23, 141 (1977).
5. G. L. Nyberg and N. V. Richardson, Surface Sci. 85, 335 (1979).
6. P. Hofmann, K. Horn and A. M. Bradshaw, Surface Sci. 105, L260 (1981).
7. F. P. Netzer and J. U. Mack, J. Chem. Phys. 79, 1017 (1983).
8. J. C. Bertolini and J. Rousseau, Surface Sci. 89, 467 (1979).
9. J. C. Bertolini, J. Massardier and B. Tardy, J. Chim, Phys. 78, 939 (1981).
10. J. Massardier, B. Tardy, M. Abon and J. C. Bertolini, Surface Sci. 126, 154 (1983).
11. J. C. Bertolini, G. Dalmai-Imelik and J. Rousseau, Surface Sci. 67, 478 (1977).
12. Ph. Avouris and J. E. Demuth, J. Chem, Phys. 75, 4783 (1981).
13. S. Lehwald, H. Ibach and J. E. Demuth, Surface Sci. 78, 577 (1978).
14. M. Surman, S. R. Bare, P. Hofmann, and D. A. King, Surface Sci. 126, 349 (1983).
15. D. M. Haaland, Surface Sci. 102, 405 (1981).
16. D. M Haaland, Surface Sci. 111, 555 (1981).

17. H. Jobic, J. Tomkinson, J. P. Candy, P Fouilloux, and A. J. Renouprez, Surface Sci. 95, 496 (1980).

18. C. M. Friend and E. L. Muetterties, J. Am. Chem. Soc. 103, 773 (1981).

19. M.-C. Tsai and E. L. Muetterties, J. Am. Chem. Soc. 104, 2534 (1982).

20. M.-C. Tsai and E. L. Muetterties, J. Phys. Chem. 86, 5067 (1982).

21. A. L. Cabrera, N. D. Spencer, E. Kozak, P. W. Davies, and G. A. Somorjai, Rev. Sci. Instrum. 53, 1888 (1982).

22. H. Froitzheim, H. Ibach and S. Lehwald, Rev. Sci. Instrum. 46, 1325 (1975).

23. J. E. Katz, P. W. Davies, J. E. Crowell and G. A. Somorjai, Rev. Sci. Instrum. 53, 785 (1982).

24. S. Semancik, G. L. Haller and J. T. Yates, Jr., Appl. Surface Sci. 10, 133 (1982).

25. R.-F. Lin, R. J. Koestner, M. A. Van Hove and G. A. Somorjai, Surface Sci, in press.

26. H. Ibach and G. A. Somorjai, Appl. Surface Sci. 3, 293 (1979).

27. H. F. Efner, D. E. Tevault, W. B. Fox and R. R. Smardzewski, J. Organomet. Chem. 146, 45 (1978).

28. T. Shimanouchi, Tables of Molecular Vibrational Frquencies, Consolidated Volume I, NSRDS-NBS39; Vol. II, J. Chem. Ref. Data 6, 993 (1977).

29. R. D. Mair and D. F. Hornig, J. Chem. Phys. 17, 1236 (1949).

30. H. Ibach and D. L. Mills, Electron Energy Loss Spectroscopy and Surface Vibrations, Academic Press, New York, 1982.

31. J. E. Demuth, K. Christmann and P. N. Sanda, Chem. Phys. Lett. 76, 201 (1980).

32. P. C. Stair and G. A. Somorjai, J. Chem. Phys. 67, 4361 (1977).

33. J. A. Gates and L. L. Kesmodel, J. Chem. Phys. 76, 4281 (1982).

34. N. V. Richardson, Surface Sci. 87, 622 (1979).

35. H. Ibach and S. Lehwald, J. Vac. Sci. Technol. 15, 407 (1978).

36. J. C. Bertolini, J. Massardier, and G. Dalmai-Imelik, J. Chem. Soc. Faraday Trans. I 74, 720 (1978).

37. W. T. Tysoe, G. L. Nyberg, and R. M. Lambert, J. Chem. Soc. Chem. Commun. 623 (1983).

38. T. M. Gentle and E. L. Muetterties, J. Phys. Chem. 87, 2469 (1983).

39. E. O. Fischer and H. P. Fritz, Angew. Chem. 73, 353 (1961).

40. P. A. Redhead, Vacuum 12, 203 (1962).

41. J. E. Demuth, H. Ibach and S. Lehwald, Phys. Rev. Lett. 40, 1044 (1978).

42. M. Brookhart and M. L. H. Green, J. Organomet. Chem. 250, 395 (1983).

43. K. J. Klabunde and H. F. Efner, J. Fluorine Chem. 4, 114 (1974).

44. G. Herzberg, Molecular Spectra and Molecular Structure II, Infrared and Raman Spectra of Polyatomic Molecules, (Van Nostrand, Princeton, N.J., 1945.

Table 1. Assignment of the observed vibrational frequencies for benzene chemisorbed in the c(2$\sqrt{3}$x4)rect structure on Rh(111) at 300K. The gas phase frequencies for C_6H_6 and C_6D_6 are included for comparison. All frequencies are given in units of cm^{-1}.

mode number [44] and representation		Mode type	Gas phase frequencies [28] $C_6H_6(C_6D_6)$	C_6H_6/C_6D_6 Ratio	Chemisorbed Frequencies $C_6H_6(C_6D_6)$	C_6H_6/C_6D_6 Ratio
ν_1	A_{1g}	CH stretch(ν_{CH})	3062(2293)	1.34	~3000(2250)*	1.33
ν_2	A_{1g}	ring stretch(ν_{CH})	992(943)	1.05	880(835)	1.05
ν_4	A_{2u}	CH bend(γ_{CH})	673(497)	1.35	~ 810(565)*	1.41
ν_9	B_{2u}	ring stretch(ν_{CC})	1310(1286)	1.02	1320(1320)	1.00
ν_{10}	B_{2u}	CH bend(δ_{CH})	1150(824)	1.40	1130(835)	1.35
ν_{13}	E_{1u}	ring str.(δ_{CC}) and deform.	1486(1335)	1.11	1420(1365)	1.04
		RhC stretch(ν_{CH})	---	--	550(550)	1.00
		RhC stretch(ν_{Rh-C})	---	--	345(330)	1.05

* Two γ_{CH} and ν_{CH} frequencies are observed under high resolution: 776 cm^{-1}, 819 cm^{-1}; 2970 cm^{-1}, 3030 cm^{-1}.

Table 2. A comparison of vibrational frequencies (cm^{-1}) observed by HREELS for benzene chemisorbed on single crystal metal surfaces with the gas phase values. Frequencies are grouped by mode assignments; original assignments, when different, are given in parentheses.

Crystal Surface	ν_{M-C}	ν_{M-C}	γ_{CH} (ν_4,A_{2u})	δ_{CH} (ν_{10},B_{2u})	δ_{CC} (ν_{13},E_{1u})	ν_{CH} (ν_1,A_{1g})	Reference
gas phase			673	1150	1486	3062	[28]
Ag(111)			675	1155	1480	3030	[12]
Ni(111)	320		730,820	1130	1430(ν_9)	3000	[13]
	290		745,845(ν_2)	1110	1420	3020	[8,9]
Ni(110)			735,845(ν_2)	1110*	1420*	3020	[9]
Ni(100)	360		750,845(ν_2)	1115	1425	3025	[8]
Rh(111)	345	550	776,819	1130	1420	3000	this study
$Pt_{10}Ni_{90}$(111)			800,845(ν_2)	1110*	1420*	3050	[9]
$Pt_{78}Ni_{22}$(111)			835,910	1130*	1385*	3010	[10]
Pt(110)	340*	565*	830*,910*	1120*	1435*	3025	[14]
Pt(111)	360	570	830,920	1130	1402(ν_9)	3000	[13]

* indicates vibrations not assigned by other authors to specific modes.

Table 3. Desorption temperatures for benzene and hydrogen from chemisorbed benzene on single crystal fcc(111) surfaces. The heats of desorption are given for relative comparisons as determined using the Redhead formula [40] assuming first order desorption kinetics and a preexponential factor of 10^{13} sec^{-1}.

crystal surface	C_6H_6 Desorption Temperature (K)	$\Delta H_d(C_6H_6)$ kcal/mole	H_2 Desorption Temperature (K)	$\Delta H_d(H_2)$ kcal/mole	References
Ni(111)	388-398	22.4-23.0	453	26.3	[18]
Rh(111)	395-415	23.2-24.4	450,670	26.6,40.1	this study
$Pt_{10}Ni_{90}$(111)	368,423	21.9,25.3	448,583	26.8,35.2	[9]
$Pt_{78}Ni_{22}$(111)	365,445	21.7,26.6	none	---	[10]
Pt(111)	373-403 473-493	21.5-23.3 27.5-28.7	543,653	31.7,38.3	[19]

Table 4. Correlation table for the symmetries of the point group D_{6h} with those of the subgroups C_{6v}, $C_{3v}(\sigma_d)$, $C_{3v}(\sigma_v)$, and C_{2v}. The vibrational frequencies for gas phase benzene are given for those modes which are active for dipole scattering using HREELS (i.e. for those modes which belong to the totally symmetric representations A_1, A' and A).

D_{6h}	C_{6v}	$C_{3v}(\sigma_d)$	$C_{3v}(\sigma_v)$	C_{2v}
A_{1g}	A_1(992,3062*)	A_1(992,3062*)	A_1(992,3062*)	A_1(992,3062*)
A_{1u}	A_2	A_2	A_2	A_2
A_{2g}	A_2	A_2	A_2	A_2
A_{2u}	A_1(673*,T_z)	A_1(673*,T_z)	A_1(673*,T_z)	A_1(673*,T_z)
B_{1g}	B_2	A_1(no vib.)	A_2	B_2
B_{1u}	B_1	A_2	A_1(1010,3068*)	B_1
B_{2g}	B_1	A_2	$A_1$995*,703*)	B_1
B_{2u}	B_2	A_1(1150*,1310)	A_2	B_2
E_{1g}	E_1	E	E	B_2+B_1
E_{1u}	E_1	E	E	B_2+B_1
E_{2g}	E_2	E	E	A_2+A_1(606,1178* 1596, 3047*)
E_{2u}	E_2	E	E	A_2+A_1(410*,975*)

* indicates modes due to C-H vibrations.

FIGURE CAPTIONS

Fig. 1. TPD spectra of (A) C_6H_6 and (B) D_2 following adsorption of (A) benzene or (B) benzene-d_6 on Rh(111) near 300K measured as a function of benzene exposure. The heating rate used was linear at 15 K/sec.

Fig. 2. Vibrational spectra obtained by HREELS in the specular direction for a saturation coverage of benzene chemisorbed on Rh(111) at 300K for a well-ordered c($2\sqrt{3}$ x 4)rect surface structure: (A) C_6H_6; (B) C_6D_6.

Fig. 3. Specular HREEL spectra obtained at 300K as a function of benzene exposure. Large variations in the scattered elastic peak intensity were observed as a function of benzene coverage: losses shown are normalized to the elastic peak intensity.

Fig. 4. Vibrational spectra for two of the ordered structures produced after benzene adsorption on Rh(111): (A) c($2\sqrt{3}$ x 4)rect, after saturation adsorption at 300K, (B) (3 x 3), after warming the layer in (A) to 393K and waiting several hours.

Fig. 5. HREEL spectra obtained at 27 cm^{-1} resolution for the ν_{CH} mode of benzene adsorbed at 310K and after heating to 390K. Spectra were recorded on an expanded scale.

Fig. 6. Absolute intensities of the vibrational frequencies observed for saturation benzene adsorption to produce the c($2\sqrt{3}$x4)rect structure on Rh(111) at 300K. The elastic peak angular dependence is shown for comparison.

Fig. 7. HREELS spectra obtained for specular and 15° off-specular (θ_i = 67.5°, θ_s = 52.5°) scattering angles for the c(2$\sqrt{3}$ x 4)rect - C_6H_6 structure.

Fig. 8. Structural model based on LEED and HREELS results for benzene adsorbed in the c(2$\sqrt{3}$ x 4)rect ordered structure. The benzene molecules are centered over hcp-type hollow sites and positioned with $C_{3v}(\sigma_d)$ symmetry. Van der Waals radii of 1.8 and 1.2 Å for C and H, respectively, are included to demonstrate packing density. The right hand benzene molecule shows the in-plane symmetric distortion preferred from dynamic LEED calculations [1]. The side view in the top panel includes possible CH bending away from the surface. A unit cell is outlined in the bottom panel.

Fig. 9. The calculated heats of desorption of molecular benzene and the adsorbed benzene ν_{CH} frequency for several metal surfaces.

Fig. 10. The clean metal work function and the adsorbed benzene ν_{CH} frequency for several metal surfaces.

APPENDIX

The surface geometry and site symmetry of an adsorbed molecule can be determined through the use of the principles of group theory in conjunction with the metal-surface dipole selection rule operable in HREELS. The symmetry assignment is made by comparing the number, frequency, and intensity of the dipole active modes observed with the correlation table of the point group for the gas phase molecule. We describe here the symmetry determination of benzene adsorbed on Rh(111) in the $c(2\sqrt{3} \times 4)$ rect structure.

First one must determine which modes of adsorbed benzene are dipole active, i.e. are due to dipole scattering. Two inelastic scattering mechanisms can be responsible for the observed electron energy loss peaks in HREELS: dipole scattering and impact scattering. Losses that are the result of dipole scattering satisfy a surface dipole selection rule and appear in a scattering lobe which is sharply peaked in the specular direction.

Impact scattering produces a broad angular scattering distribution and the losses do not satisfy the above selection rule. The contributions of the two mechanisms can be distinguished by studies of the angular dependence of the losses in HREELS. The results in Fig. 6 show that all of the observed loss peaks in Fig. 2 are dipole active. The assignment in Table 1 of these peaks to vibrational modes derived from gas phase benzene modes is made by using the isotope shift and the results of force field calculations for benzene complexes [17].

We now consider the correlation table for the symmetry point group of gas phase benzene, D_{6h}. By using the relationships between the representation of D_{6h} and its subgroups, we can predict which modes would be observed as dipole active in HREELS upon reduction of the gas phase benzene symmetry. Only those modes that belong to totally symmetric representations (A_1, A', or A) satisfy the surface dipole selection rule and are observed in dipole scattering. Gas phase benzene vibrational frequencies are given in Table 4 for those modes that have A_1, A' or A representation under the given symmetry at the surface. Six additional vibrational modes should also appear in HREELS, since the benzene molecules become fixed in space upon adsorption, removing the translational and rotational degrees of freedom. These new modes involve dipole moment changes perpendicular (A_{2u} symmetry mode T_z) and parallel (E_{1u} symmetry degenerate modes T_x and T_y) to the ring plane and may be dipole active.

Only a few D_{6h} subgroup symmetries are considered in Table 4. The strong intensity of the dipole active γ_{CH} (A_{2u}) mode and the weak intensity of the other dipole active modes that involve dipole moment changes in the ring plane indicate that the molecular ring plane is parallel to the metal surface and the in-plane modes are effectively screened by the metal surface. This general orientation makes only a few symmetries possible, as indicated in Table 4.

Symmetry groups lower than C_{3v} can be ruled out, since only seven vibrational modes are observed to be dipole active. Clearly, the number and frequency of the observed dipole active modes favor the

C_{3v} point groups. The 1130 and 1320 cm^{-1} dipole active modes lead to the conclusion that the adsorption site symmetry is C_{3v} (σ_d). The appearance of the 1420 cm^{-1} mode (ν_{13}, E_{1u}) to be dipole active in Fig. 6 is not explained by this symmetry assignment. Possibly, several unresolved impact scattering losses which have small differences in their angular dependences comprise this peak.

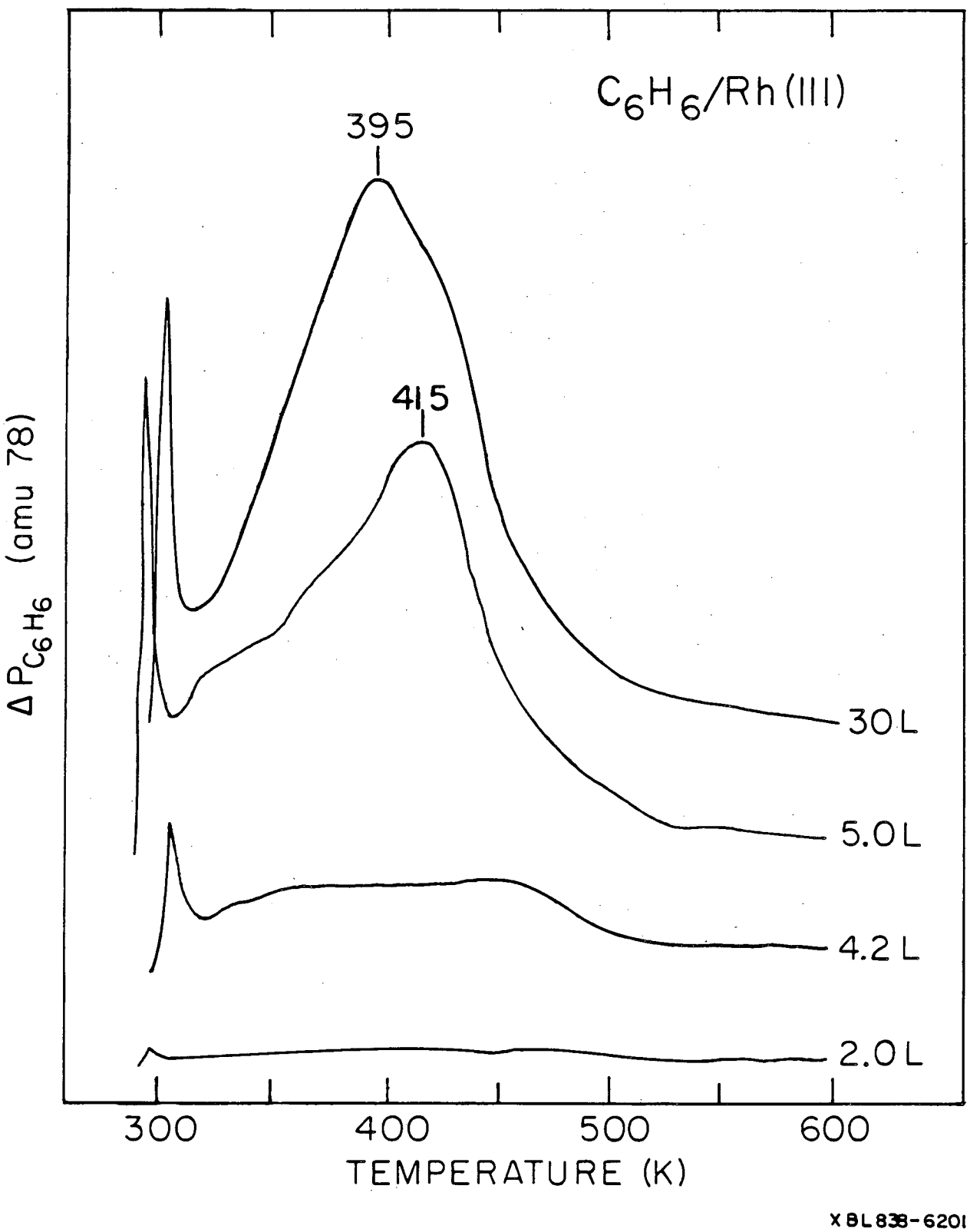
C6H6/Rh(III)
395
415
30 L
5.0 L
4.2 L
2.0 L
ΔPC6H6 (amu 78)
300
400
500
600
TEMPERATURE (K)
XBL838-6201

Fig. 1A

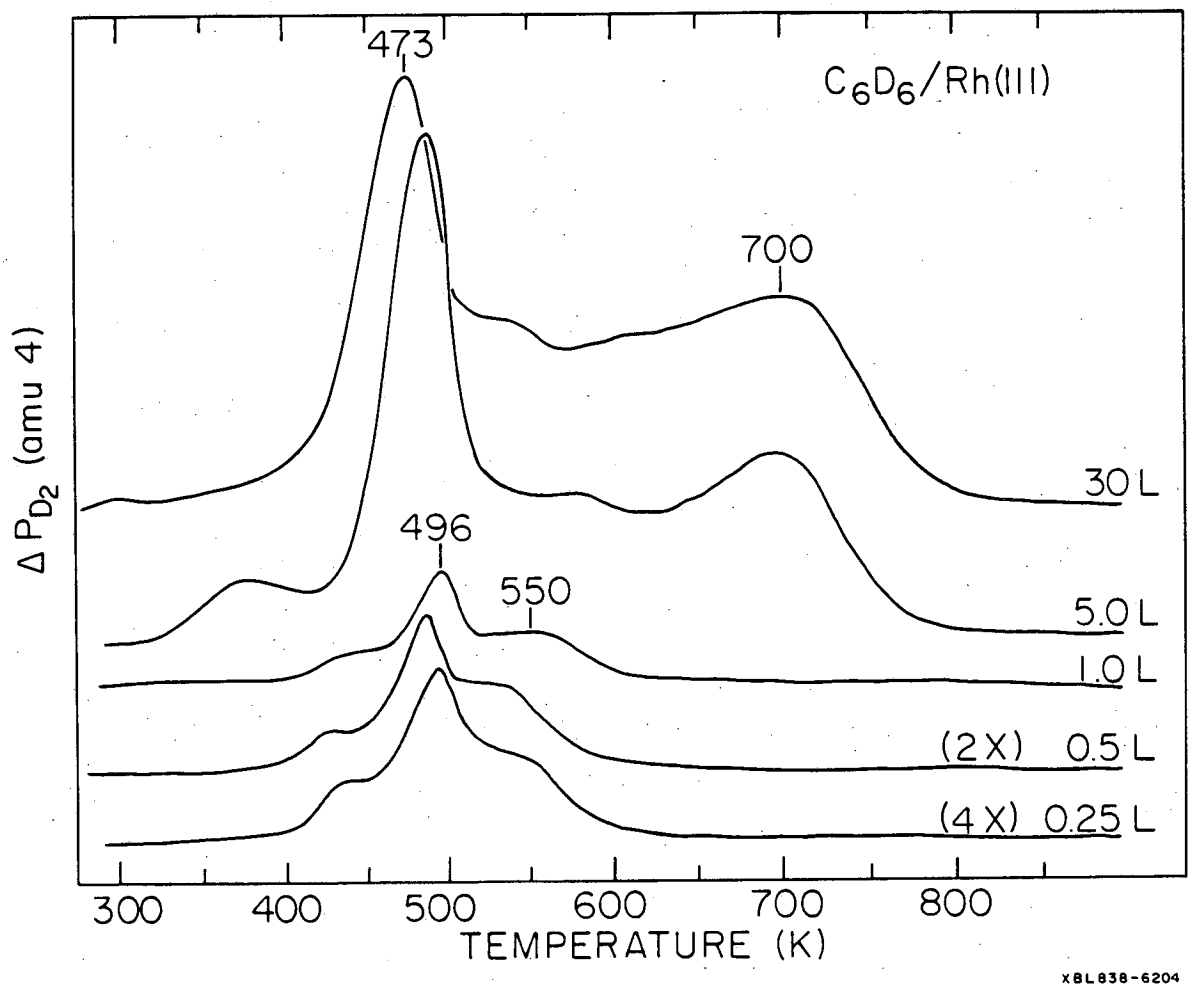
473
700
496
550
C_6D_6/Rh(111)
30 L
5.0 L
1.0 L
(2X) 0.5 L
(4X) 0.25 L
ΔP_{D_2} (amu 4)
300
400
500
600
700
800
TEMPERATURE (K)
XBL838-6204

Fig. 1B

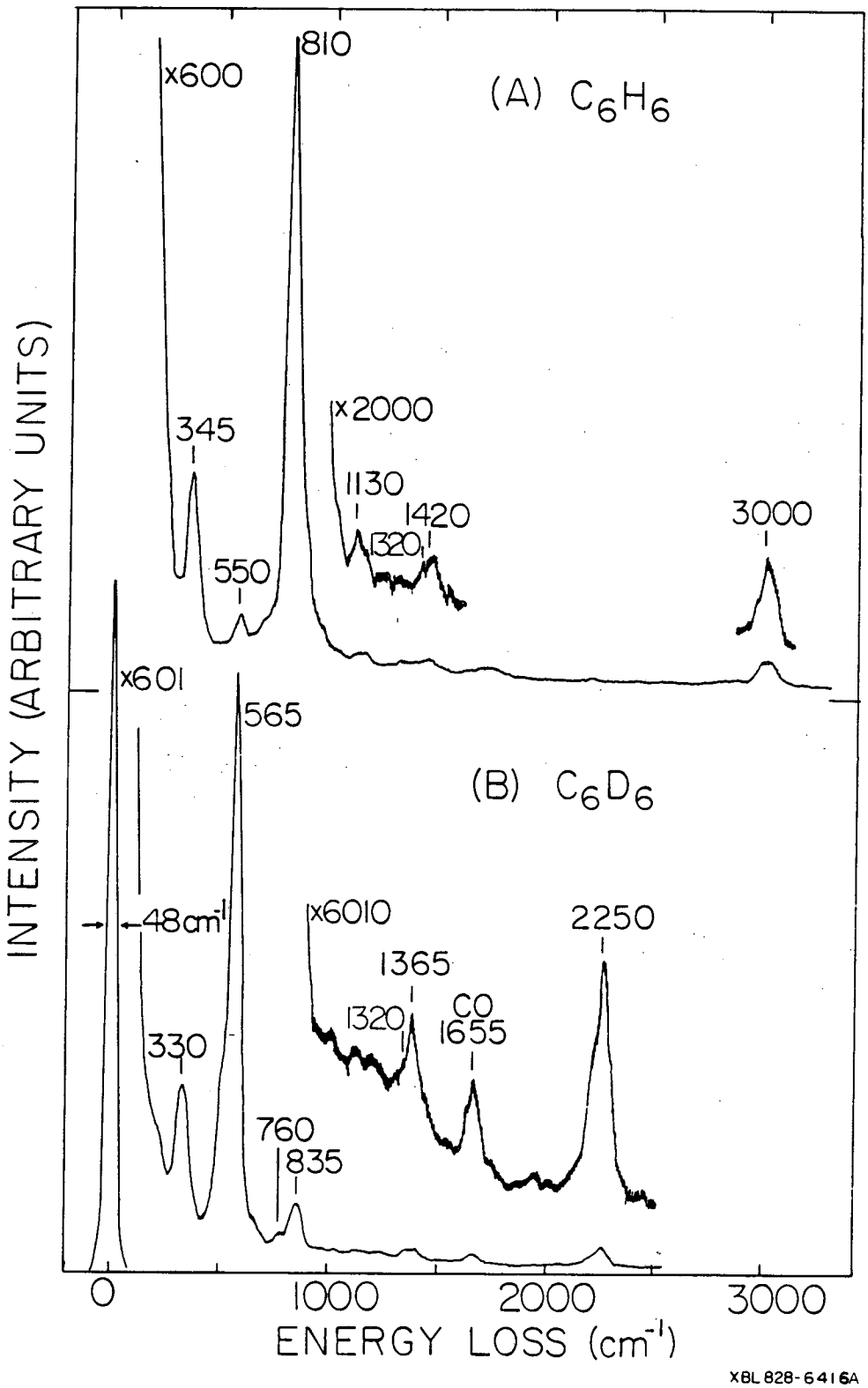
x600
810
(A) C_6H_6
345
x2000
1130
1420
1320
3000
550
x601
565
(B) C_6D_6
48cm⁻¹
x6010
2250
1365
1320
CO
1655
330
760
835
INTENSITY (ARBITRARY UNITS)
0
1000
2000
3000
ENERGY LOSS (cm⁻¹)
XBL828-6416A

Fig. 2

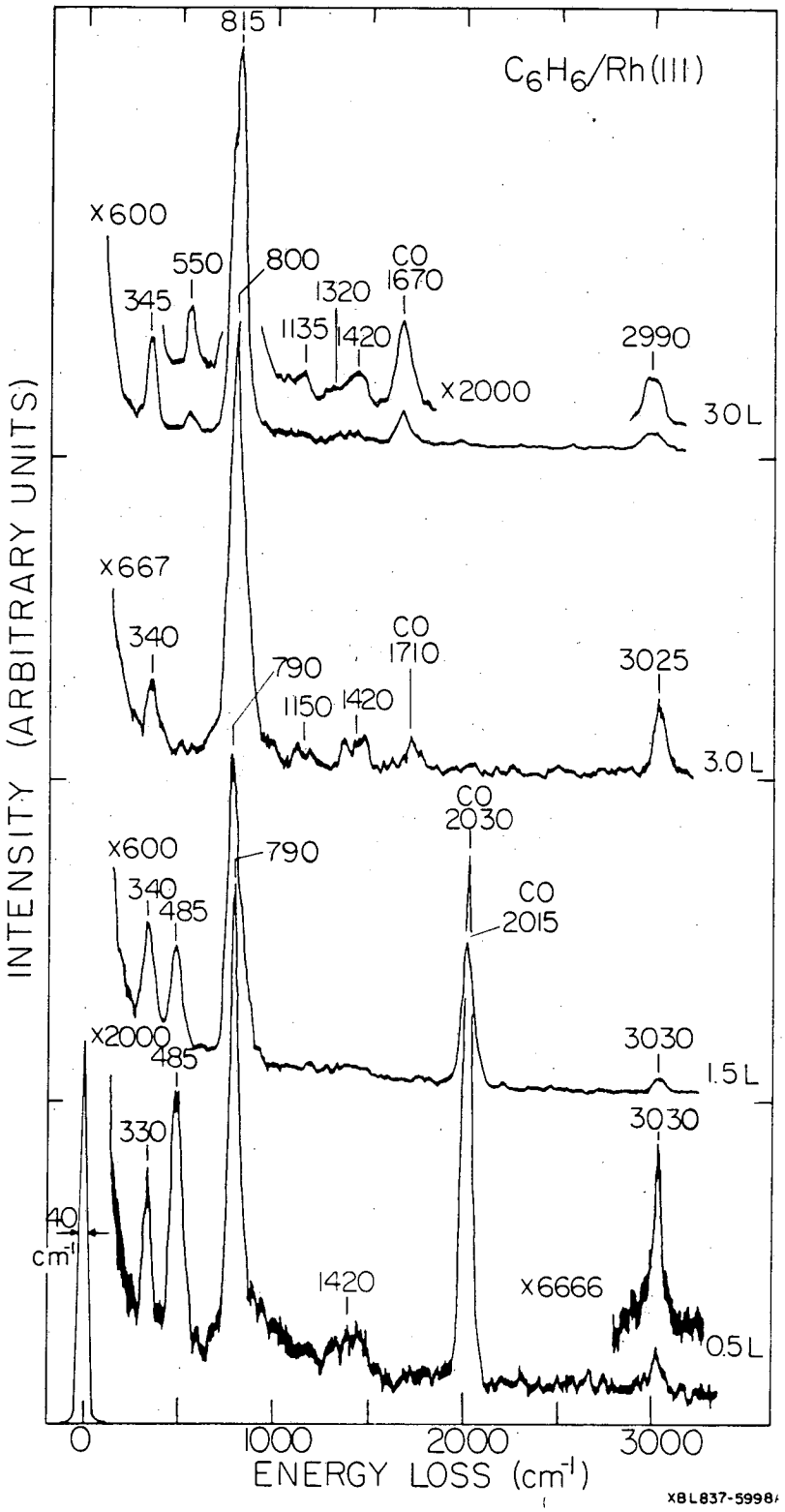
815
C_6H_6/Rh(111)
x600
550
800
CO
1670
345
1320
1135
1420
2990
x2000
3.0 L
x667
340
CO
1710
790
3025
1150
1420
3.0 L
CO
2030
x600
790
340
485
CO
2015
x2000
485
3030
1.5 L
330
3030
40
cm⁻¹
1420
x6666
0.5 L
INTENSITY (ARBITRARY UNITS)
0
1000
2000
3000
ENERGY LOSS (cm⁻¹)
XBL837-5998

Fig. 3

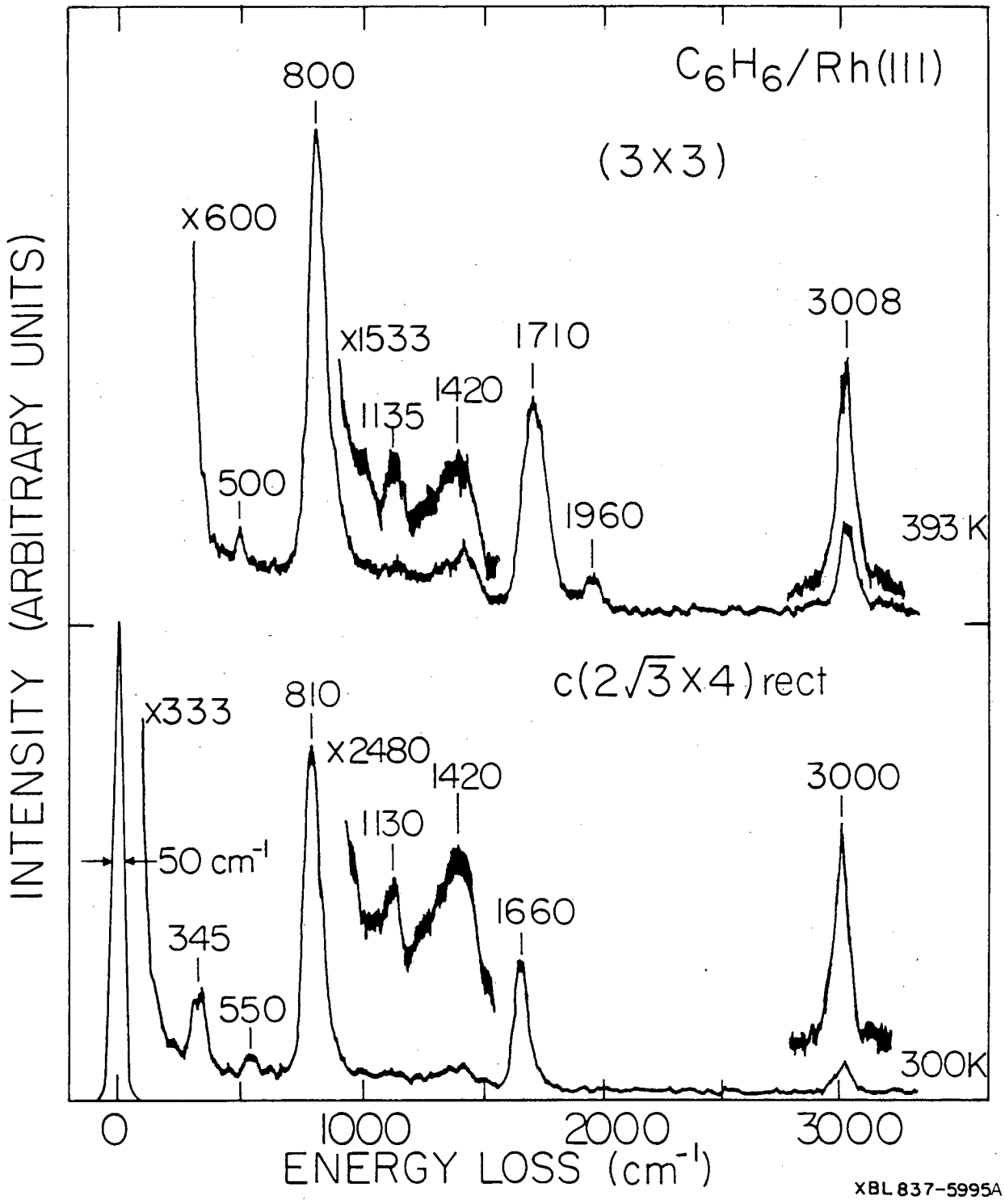
C6H6/Rh(111)
(3x3)
800
x600
500
x1533
1135
1420
1710
1960
3008
393 K
c(2√3x4) rect
x333
810
x2480
1420
1130
1660
3000
50 cm-1
345
550
300K
INTENSITY (ARBITRARY UNITS)
0
1000
2000
3000
ENERGY LOSS (cm-1)
XBL 837-5995A

Fig. 4

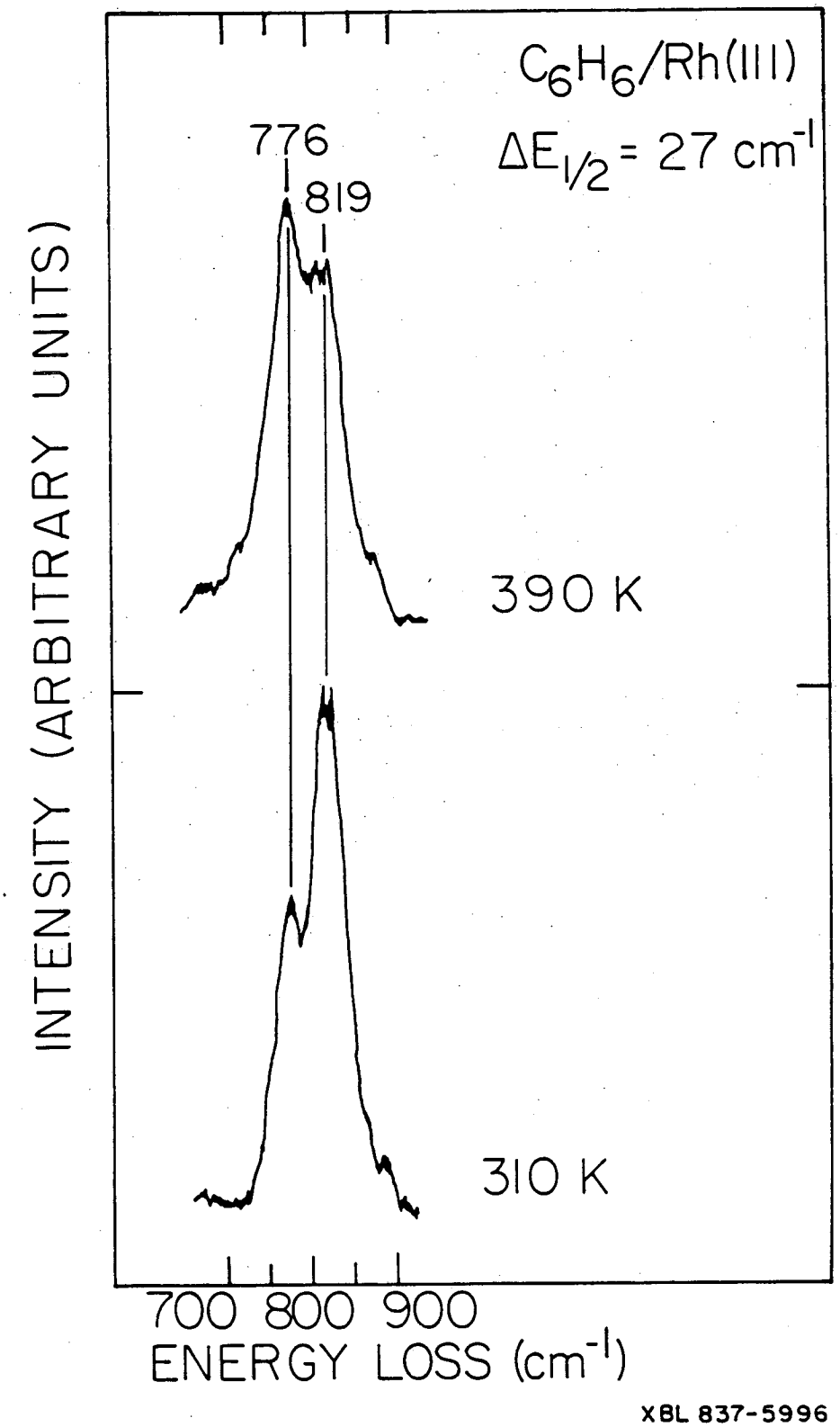
C6H6/Rh(111)
ΔE1/2 = 27 cm-1
776
819
390 K
310 K
INTENSITY (ARBITRARY UNITS)
700 800 900
ENERGY LOSS (cm-1)
XBL 837-5996

Fig. 5

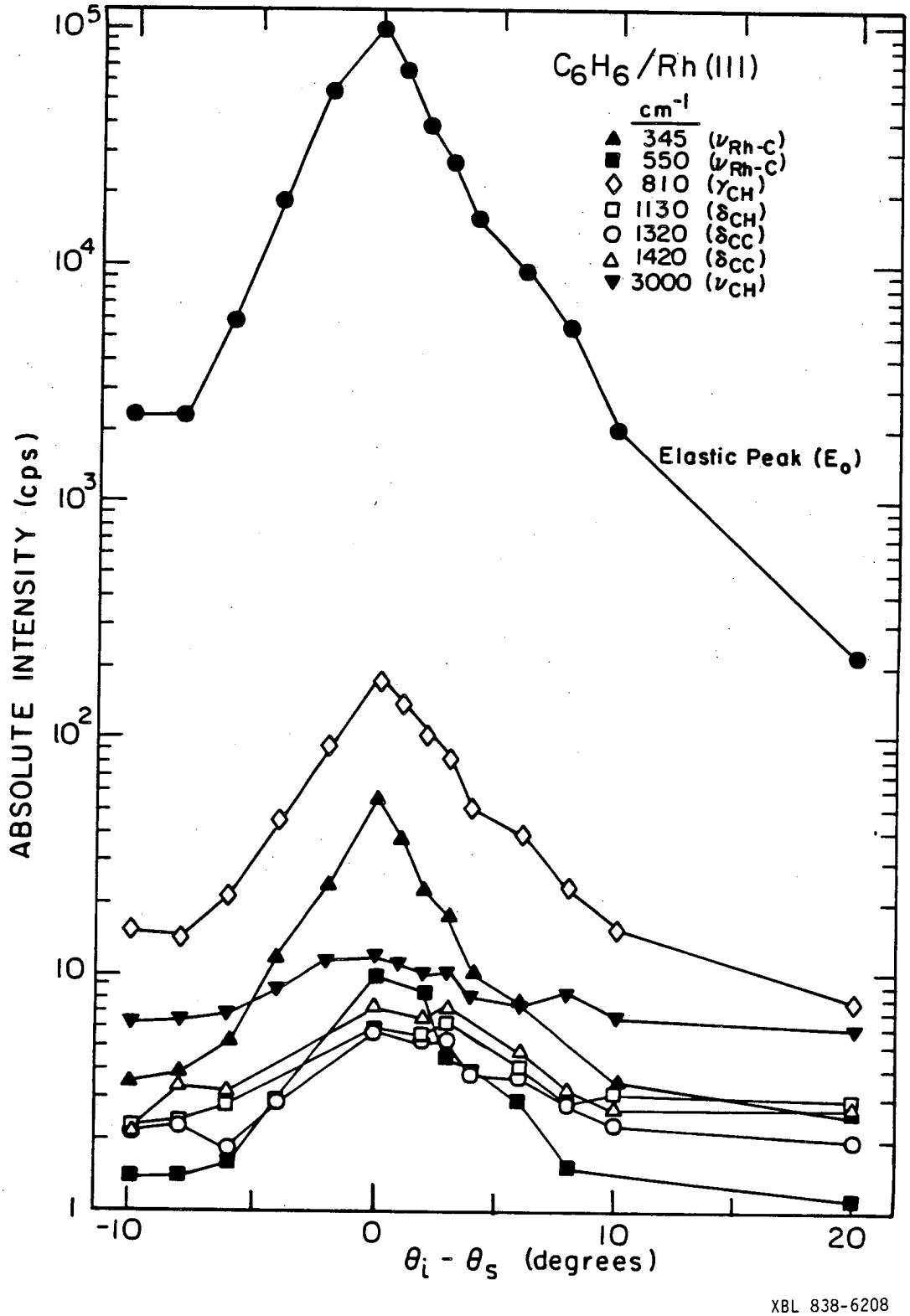
$C_6H_6/Rh(111)$
cm⁻¹
345 (ν_{Rh-C})
550 (ν_{Rh-C})
810 (γ_{CH})
1130 (δ_{CH})
1320 (δ_{CC})
1420 (δ_{CC})
3000 (ν_{CH})
Elastic Peak (E_o)
ABSOLUTE INTENSITY (cps)
10^5
10^4
10^3
10^2
10
1
-10
0
10
20
$\theta_i - \theta_s$ (degrees)
XBL 838-6208

Fig. 6

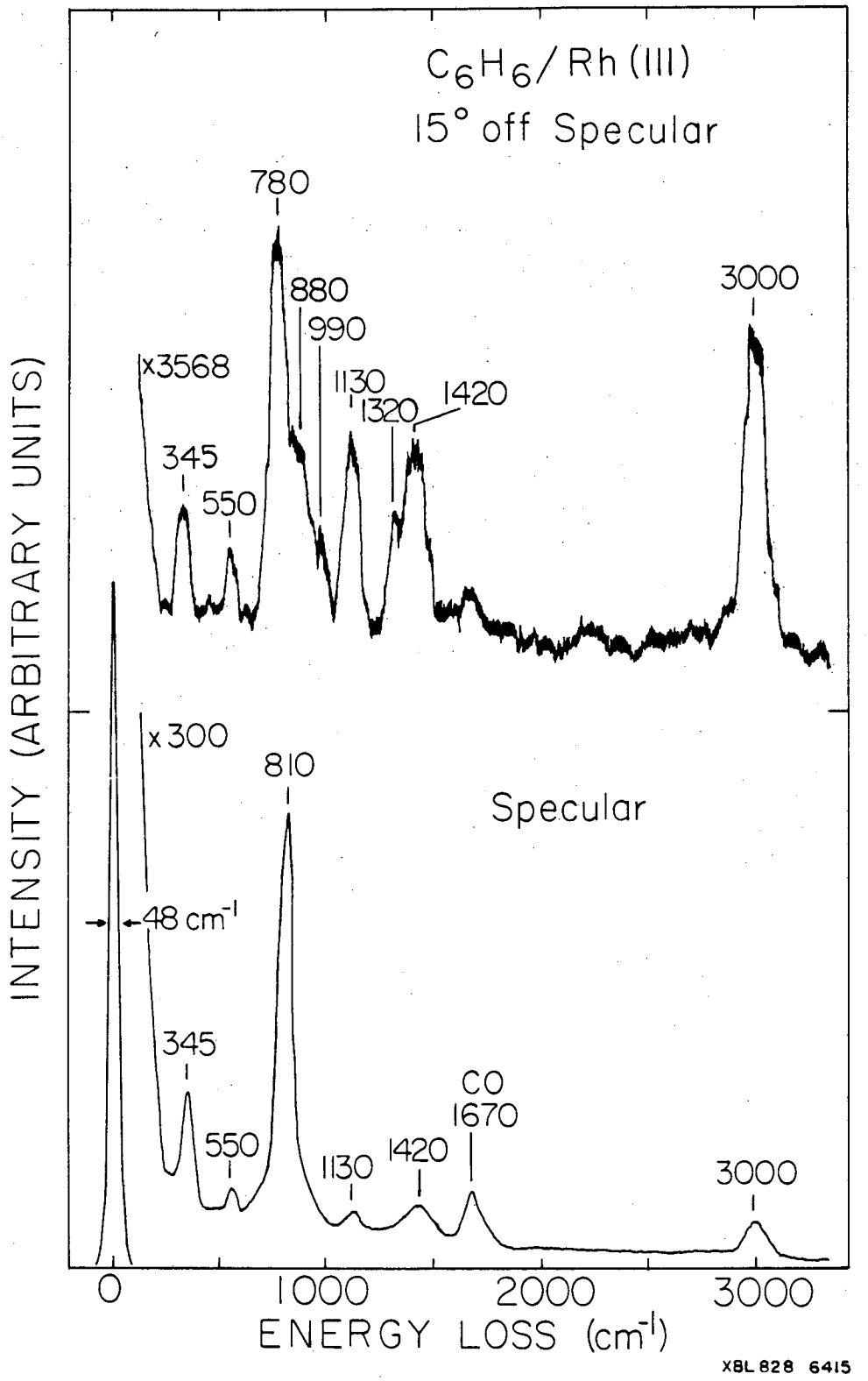
C6H6/Rh(111)
15° off Specular
780
880
990
1130
1320
1420
3000
x3568
345
550
x300
810
Specular
48 cm-1
345
550
1130
1420
CO
1670
3000
INTENSITY (ARBITRARY UNITS)
0
1000
2000
3000
ENERGY LOSS (cm-1)
XBL 828 6415

Fig. 7

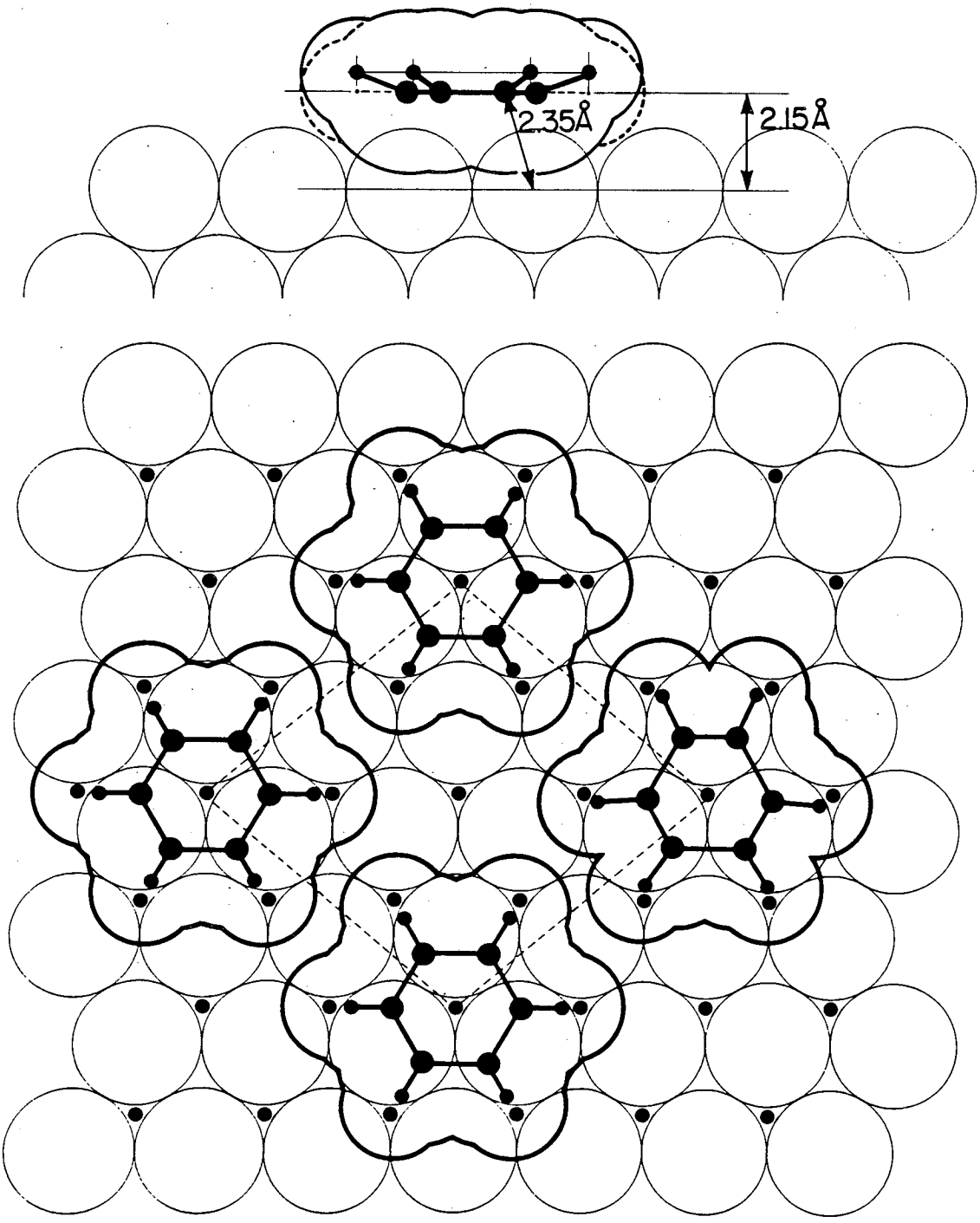

$Rh(111)-\begin{pmatrix} 3 & 1 \\ 1 & 3 \end{pmatrix} C_6H_6$

XBL 835-198

Fig. 8

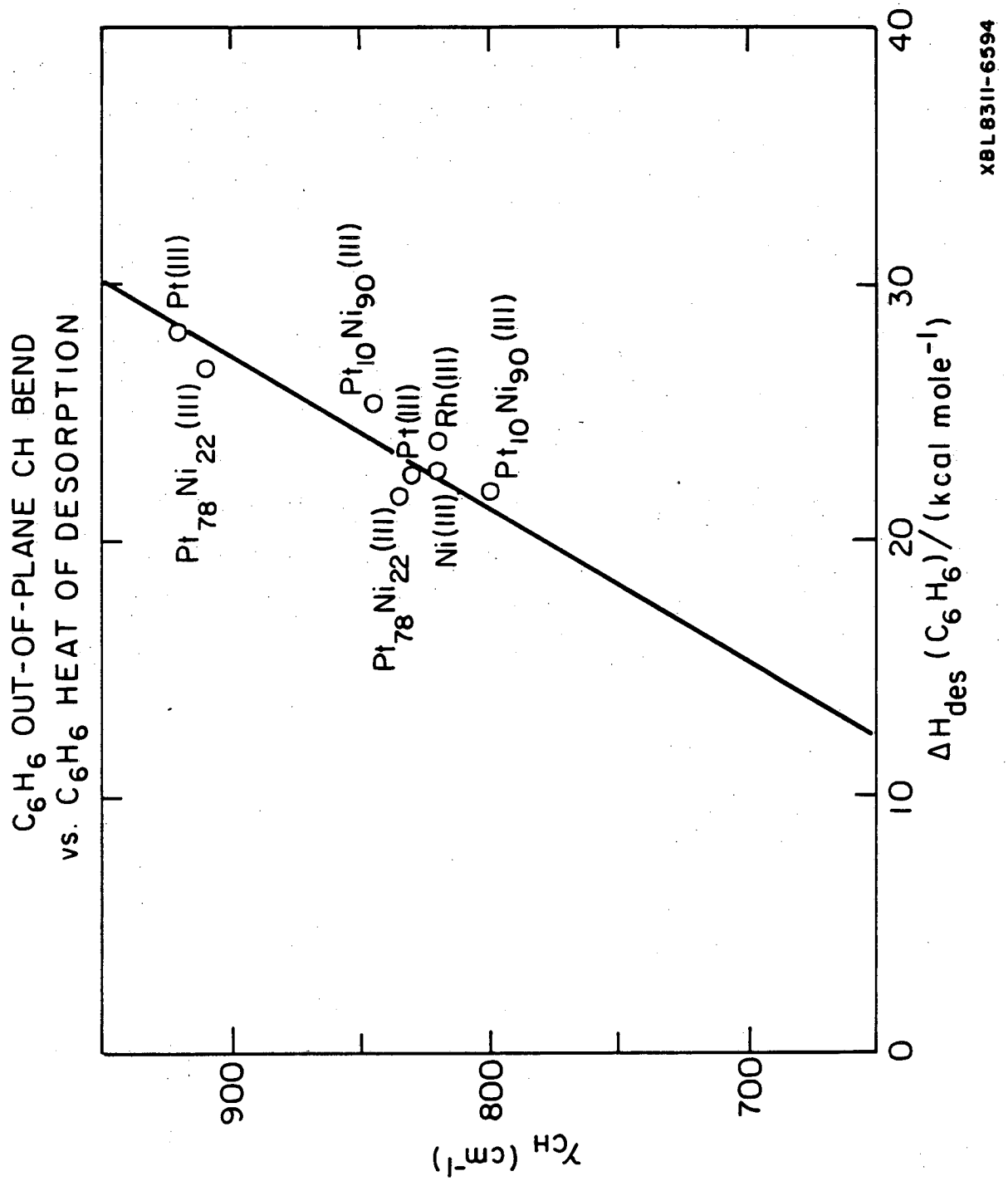
C6H6 OUT-OF-PLANE CH BEND
vs. C6H6 HEAT OF DESORPTION
γCH (cm-1)
ΔHdes (C6H6) / (kcal mole-1)
900
800
700
0
10
20
30
40
Pt(III)
Pt78Ni22(III)
Pt10Ni90(III)
Pt78Ni22(III)
Pt(III)
Rh(III)
Ni(III)
Pt10Ni90(III)
XBL8311-6594

Fig. 9

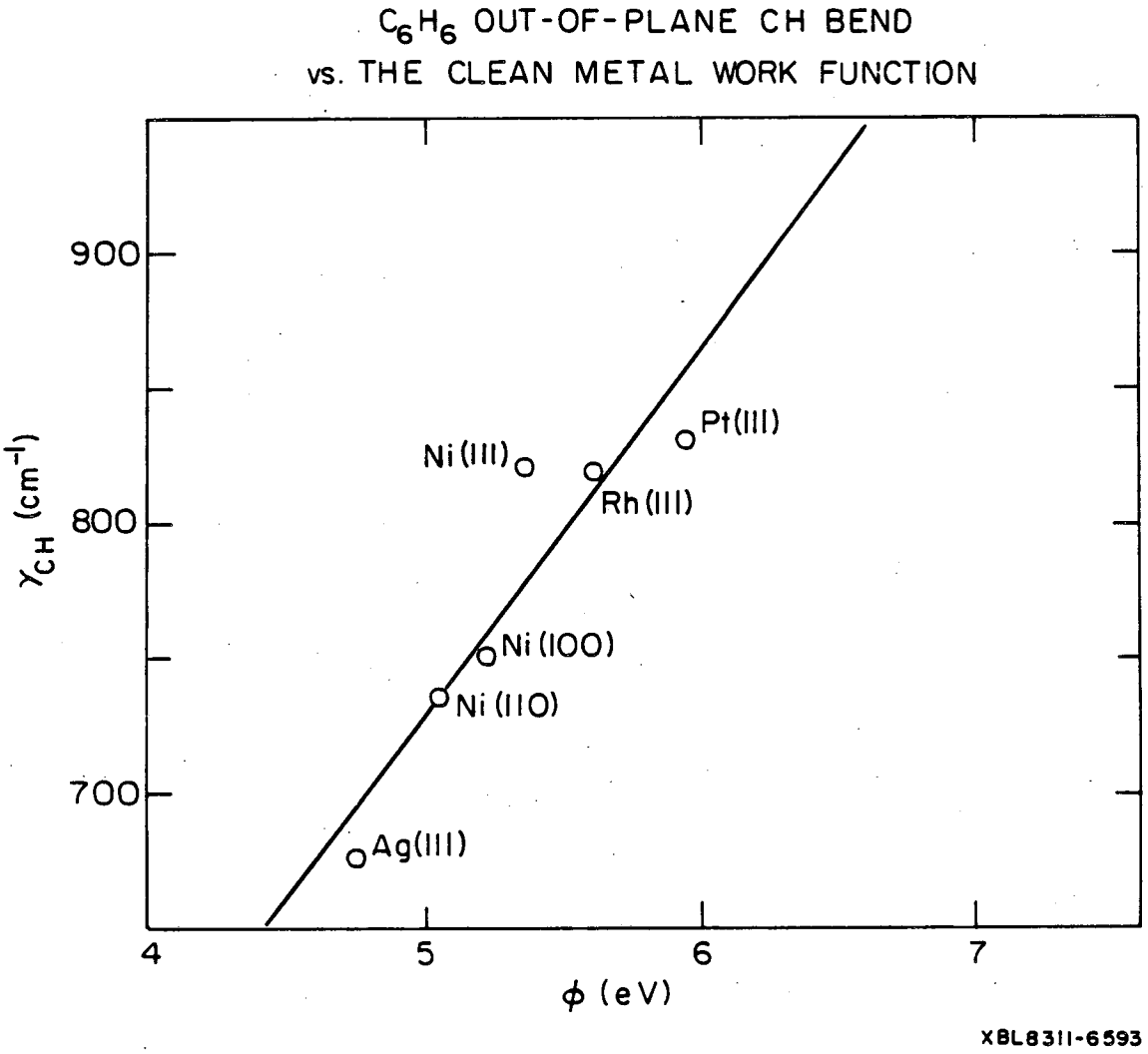
C6H6 OUT-OF-PLANE CH BEND
vs. THE CLEAN METAL WORK FUNCTION
900
800
700
γCH (cm-1)
Pt(111)
Ni(111)
Rh(111)
Ni(100)
Ni(110)
Ag(111)
4
5
6
7
φ (eV)
XBL8311-6593

Fig. 10

TECHNICAL INFORMATION DEPARTMENT
LAWRENCE BERKELEY LABORATORY
UNIVERSITY OF CALIFORNIA
BERKELEY, CALIFORNIA 94720